J Mater Sci: Mater Med (2006) 17:1245–1254
DOI 10.1007/s10856-006-0598-4

In-vitro study of the spontaneous calcification of PHEMA-based hydrogels in simulated body fluid

Zainuddin · D. J. T. Hill · A. K. Whittaker · T. V. Chirila

Received: 24 August 2005 / Accepted: 4 January 2006

Abstract *In-vitro* calcification of poly(2-hydroxyethyl methacrylate) (PHEMA)-based hydrogels in simulated body fluid (SBF) under a steady/batch system without agitation or stirring the solutions has been investigated. It was noted that the formation of calcium phosphate (CaP) deposits primarily proceeded through spontaneous precipitation. The CaP deposits were found both on the surface and inside the hydrogels. It appears that the effect of chemical structure or reducing the relative number of oxygen atoms in the copolymers on the degree of calcification was only important at the early stage of calcification. The morphology of the CaP deposits was observed to be spherical aggregates with a thickness of the CaP layer less than 0.5 μm. Additionally, the CaP deposits were found to be poorly crystalline or to have nano-size crystals, or to exist mostly as an amorphous phase. Characterization of the CaP phases in the deposits revealed that the deposits were comprised mainly of whitlockite [$Ca_9MgH(PO_4)_7$] type apatite and DCPD ($CaHPO_4 \cdot 2H_2O$) as the precursors of hydroxyapatite [$Ca_{10}(PO_4)_6(OH)_2$]. The presence of carbonate in the deposits was also detected during the calcification of PHEMA based hydrogels in SBF solution.

Zainuddin (✉) · D. J. T. Hill
Department of Chemistry, The University of Queensland,
St. Lucia, Brisbane Qld 4072, Australia
s4001393@student.uq.edu.au; z.zainuddin@uq.edu.au

A. K. Whittaker
Centre for Magnetic Resonance, The University of Queensland,
St. Lucia, Brisbane Qld 4072, Australia

T. V. Chirila
Prevent Blindness Foundation, Queensland Eye Institute,
41 Annerley Road, South Brisbane Qld 4101, Australia

1 Introduction

The process of calcification of implants or tissues has long been studied and well described, but the molecular mechanism of calcification is less well understood [1, 2]. This is probably because the mechanism of calcification is complex in the presence of biologically active macromolecules, including enzymes. Therefore, the mechanism of calcification of model implants has been studied using an abiotic media. This equilibration procedure allows simpler evaluation of the nature of calcification processes in macromolecular matrices, but it is still necessary to compare the results obtained with *in vivo* studies for complete evaluation of the phenomena. The use of abiotic calcifying media which simulate body fluids, and contain ion concentrations nearly equal to those of the inorganic constituents of human blood plasma, was first introduced by Kokubo [3]. The author found that even in a cell-free simulated body fluid (SBF) system a "bone-like" apatite can be formed on bioactive materials, such as bioglasses and glass-ceramics. Since then, SBF has been widely used for assessment of the bioactivity of various materials and the formation of bone-like apatite on various implants *in vitro*.

In the case of calcification of polymeric hydrogels, it was noticed that unlike other synthetic biomaterials, hydrogels undergo calcification not only on the surface, but also frequently inside the hydrogels [4–6]. As hydrogels have intrinsic elasticity and water retention ability, they resemble natural hydrogels, such as collagen matrices, which are known to be associated with calcification of various tissues, including bone. Another important feature of hydrogels that can be related to the calcification of tissues or bone is that they can be assembled in three-dimensional form with multiple functional domains, such as groups that mimic the matrix proteins which regulate mineral growth. Based on this analogy, it is

quite reasonable to attempt to elucidate the mechanism of calcification in tissues and bone by studying the calcification of a hydrogel model.

Previous researchers [7, 8] reported that proteins or peptides in body fluids play a significant role in the calcification of hydrogels. They observed that albumin adsorbed onto hydrogels limited the calcification on the surface, while low molecular weight peptide, particularly lysozyme, accounted for the calcification inside the hydrogels. These processes suggest that organic constituents mediate the calcification process. Hence, it would be expected that during *in-vitro* (SBF) incubation the mechanism of calcification of hydrogels would be altered, as there would be no an organic layer to mask the functional groups of the hydrogels.

Therefore, the mechanism of calcification of hydrogels in SBF solutions may be proposed to proceed through the following stages. Initial chelation of Ca^{2+} ions occurs, in which the ions bind to hydrophilic/hydrophobic groups of the polymer, forming Ca-polymer complexes. The chelates formed will act as nucleation centres to which phosphate ions are attracted and form crystal nodules. The crystal nodules continue to grow spontaneously by attracting further Ca^{2+} and PO_4^{3-} ions from the SBF solutions until all charges are neutralized and finally a calcium phosphate (CaP) crystal precipitates. Often, many of these growing crystals fail to reach maturation stages and undergo dissolution. However, under supersaturated conditions, as is the case in SBF solution, calcium phosphate is likely to form as an amorphous precipitate. There is much evidence that biomaterials-associated calcification (BAC) involves the formation of calcium phosphate phases having compositions similar to that of hydroxyapatite [$Ca_{10}(PO_4)_6(OH)_2$] of bone, but of poorer crystallinity [9, 10]. This suggests that the amorphous precipitation process is prevalent in BAC.

In a previous report [2], it was mentioned that in addition to precipitation through heterogeneous nucleation, the mechanism for calcification in abiotic media could be attributed to the concentration gradient for the ionic solutes when the solution diffuses into the hydrogel network, leading to local supersaturation and spontaneous precipitation through homogeneous nucleation. This latter phenomenon appears to be plausible based on our very recent observation of the effects of the solute species on the enhancement of local supersaturation [11].

The current work was aimed to further improve our understanding of the mechanism of calcification on/in PHEMA-based hydrogels, and to identify the CaP phases formed during the calcification in SBF solutions. Additionally, to support our earlier hypothesis [11, 12], the effects of copolymer structure and reducing the relative number of oxygen atoms in the copolymer on the formation of CaP deposits were also investigated.

2 Experimental procedure

2.1 Materials

2-Hydroxyethyl methacrylate (HEMA), stabilized with 300 ppm of monomethylether hydroquinone, MEHQ, was obtained from SIGMA and was purified by vacuum distillation at 63°C and 2–5 mmHg. After purification, the HEMA was found by GC analysis to contain approximately 0.05 mol% ethyleneglycol dimethacrylate (EGDMA) as an impurity. Ethyl methacrylate (EMA), stabilized with 15 ppm MEHQ; styrene (St), stabilized with 10–15 ppm 4-tertiary butyl catechol; N-vinylpyrrolidone (NVP), stabilized with 0.01% NaOH, were supplied by ALDRICH Co. Ltd. and purified by vacuum distillation (2–5 mmHg).

Benzoyl peroxide (BPO) was obtained from SIGMA and twice re-crystallized from a mixture of chloroform—methanol [13]. The crystals were dried under vacuum to constant weight and stored in a dark container at ca. 4°C.

Calcium chloride dihydrate ($CaCl_2{\cdot}2H_2O$), calcium atomic absorption standard solution (containing 1,000 μg/mL of Ca^{2+} ion in 0.01% HCl), hydrochloric acid (HCl), magnesium chloride hexahydrate ($MgCl_2{\cdot}6H_2O$), potassium chloride (KCl), potassium hydrogen phosphate (K_2HPO_4), potassium hydroxide (KOH), sodium chloride (NaCl), sodium bicarbonate ($NaHCO_3$), sodium phosphate (Na_2SO_4), strontium chloride ($SrCl_2$) and trishydroxymethyl aminomethane [$(CH_2OH)_3CNH_2$)] were all analytical grade and used as received.

2.2 Synthesis of PHEMA-based hydrogels

HEMA, or HEMA together with a comonomer, was mixed with initiator (BPO) 0.05 M, and the resulting solution was poured into a silicone tube with an inner diameter ≈0.3 cm and placed into a glass container that could be evacuated. After the container was purged with nitrogen gas to remove oxygen for one hour, it was gently evacuated to a pressure of 2–5 mmHg. Polymerization was carried out in a vacuum oven (150 mmHg) for 20 h at 50°C, followed by a post-cure treatment for 2 h at 80°C. This led to complete conversion of the monomer, as indicated by the loss of the NIR peak at 6170 cm^{-1} which is characteristic of the monomer double bonds. After preparation, the cylinders were cut to a 2.5 cm length, soaked in methanol to equilibrium swelling, and then swollen in Millipore water (18.2 MΩcm) until substantially all the methanol was replaced by water (very small traces of MeOH were detected by NMR). These swelling steps allow the samples to attain an equilibrium water content (EWC) nearly the same for all of the samples. Prior to calcification experiments, all of the samples were equilibrated in Millipore water at 37°C for about 2 weeks. The EWC of the PHEMA-based cylindrical hydrogels were calculated from

the weights of the hydrated samples at equilibrium and the weight of the dry polymers.

2.3 *In-vitro* calcification

The cylindrical samples were each immersed in glass vials containing 20 mL of SBF solution and incubated in an oven at $37 \pm 0.5^{\circ}$C for certain periods of time. The SBF solutions were prepared according to the procedures described by Tas [14] and Saiz et al. [15], and were changed once every week. After completion of the experiments, the samples were rinsed rigorously with Millipore water. Except for light microscopy, all samples were dried and placed in plastic vials and stored in a desiccator.

2.4 Attenuated total reflectance fourier transform infrared (ATR-FTIR) analysis

An ATR sampling technique for infrared spectrometry was used to detect the formation of calcium salts on the surface of the cylindrical hydrogels. This technique is simple, as the specimen can be measured directly without any additional treatment. However, good contact between the sample and the internal reflection element (IRE) is required. For characterization of calcification within the bulk of the samples, a potassium bromide (KBr) disk technique was employed. In this case, the calcified samples were prepared in powder form using a freezer-mill and diluted with KBr (1:50). A mixture of the sample and KBr was placed in a special die and a disk was pressed using approximately 10^4 kg pressure. The spectra were acquired in the region of 400–4000 cm^{-1} either using a Nicolet 870 Nexus FT-IR with a diamond crystal as the ATR objective or a Perkin-Elmer FT-IR 1600 spectrometer at a resolution of 8 cm^{-1} using 64 scans.

2.5 X-ray photoelectron spectroscopy (XPS) analysis

The XPS data were acquired using a Kratos Axis ULTRA X-ray Photoelectron Spectrometer incorporating a 165 mm hemispherical electron energy analyzer. The source of X-ray incident radiation was Mg Kα (1253.6 eV) at 150 W (15 kV, 10 mA). Survey (wide) scans were taken at an analyser pass energy of 160 eV and multiplex (narrow) high resolution scans at 20 eV. The base pressure in the analysis chamber was 1.0×10^{-7} Pa and during sample analysis was 1.0×10^{-6} Pa. For quantification of the Mg peaks, the Mg 2s peak has been used, as the Mg 2p peak cannot be used because there is a heavy interference from the Ca 3s peak at binding energy (BE) of ca. 45 eV.

2.6 X-ray diffraction (XRD) analysis

The CaP deposits were separated from the polymer by scraping the surface of the sample. In using this procedure, it was not possible to avoid the inclusion of some of the matrix polymer. The sample was then ground to fine powder prior to the XRD measurement. The XRD spectra were acquired using a Bruker AXS D8 Advance XRD with an X-ray energy of 1200 W (40 kV, 30 mA) and a scanning speed of 24.5 s per step with an increment 0.02° over a 2-theta range of 2 to 70°.

2.7 Scanning electron microscopy and energy dispersive X-ray spectroscopy (SEM/EDS) analysis

Prior to SEM or EDS analysis, the samples were coated with platinum or carbon. The SEM micrographs were taken using a JEOL 6400F SEM with an acceleration voltage for the electrons of 5 kV. For X-ray microelemental analysis a JEOL 6460LA EDS with an electron acceleration voltage of 15 kV was used.

2.8 Light microscopy (LM) analysis

Both control and calcified samples were first stained with alizarin red by dipping them in a 1%wt alizarin red—alkaline solution at room temperature for one day. The samples were then washed with distilled water, soaked in 0.5% KOH solution until there was no further change in colour, and finally they were maintained in distilled water for at least 2 weeks prior to observation under an LM (OLYMPUS SZH10) incorporating a NIKON digital camera.

3 Results and discussion

The SEM images of PHEMA shown in Fig. 1(A) to (D) after soaking in SBF solution indicate the progress of the formation of a CaP layer and the aggregation of globular deposits. The maximum average size of the spherical aggregates before they merge to form a continuous layer is less than 0.5 microns. Once the surface of the hydrogels is fully covered with a CaP layer, the mechanism of nucleation becomes independent of the polymer-calcium interaction. Thus, the formation of CaP deposits beyond the first layer will be initiated mostly through homogeneous nucleation. Under these conditions, it would be anticipated that the CaP phases formed in the upper layers of the deposits would be of the same form for all of the hydrogels. Evidence for this similarity was obtained from the SEM images of the CaP deposits formed on the PHEMA homopolymer and the copolymer samples taken after 9 weeks calcification (Fig. 1(E) to (H)). Since the morphologies of both the first and the second layers

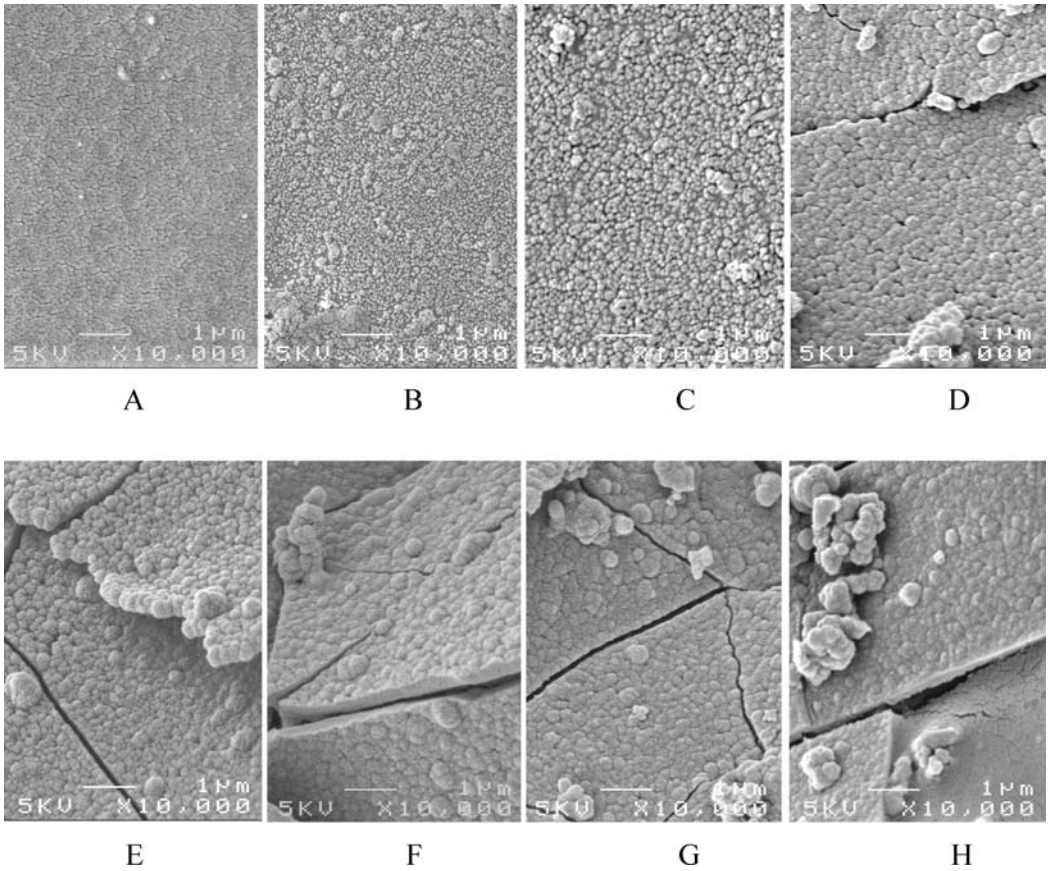

Fig. 1 SEM images of the PHEMA hydrogels before (A) and after incubation in SBF solution for 1(B), 3(C), 5(D) and 9(E) weeks, and the calcified copolymers; P(HEMA-co-EMA) (F), P(HEMA-co-NVP) (G) and P(HEMA-co-St) (H)

of the CaP deposits were found to be the same, this suggests that the formation of the apatite deposits occurs mainly through spontaneous precipitation of either nanocrystalline or amorphous CaPs, irrespective of whether the nucleation was heterogeneous or homogeneous.

Because of the nature of the heterogeneous nucleation, which occurs in the formation of the first CaP layer, this layer will be anchored to some degree to the polymer in the hydrogel, thus all of the subsequent CaP layers will also be attached strongly onto the surface of the hydrogels.

The XPS and EDS data given in Figs. 2 and 3 respectively provide strong evidence for the presence of Mg^{2+} ions in the PHEMA hydrogel after soaking in SBF solution. The detection of traces of Cl^- and Na^+ in the EDS spectra arose because EDS involves the use of a much higher energy radiation than that used in XPS. As a result, the electrons penetrate deeper into the matrix, leading to the generation of X-rays from up to a few microns below the surface. At this depth not all of the Na^+ and Cl^- ions present in the SBF solution are completely washed out during rinsing of the samples. As the apatite deposits formed on the surface of the hydrogels contain Mg^{2+} ions and have a similar morphology to that observed by Abbona and Angela [16], who obtained apatite precipitates from solutions with an equal concentration of calcium and phosphate (5 mM), the deposits are composed of mainly whitlockite-type apatite [$Ca_9MgH(PO_4)_7$]

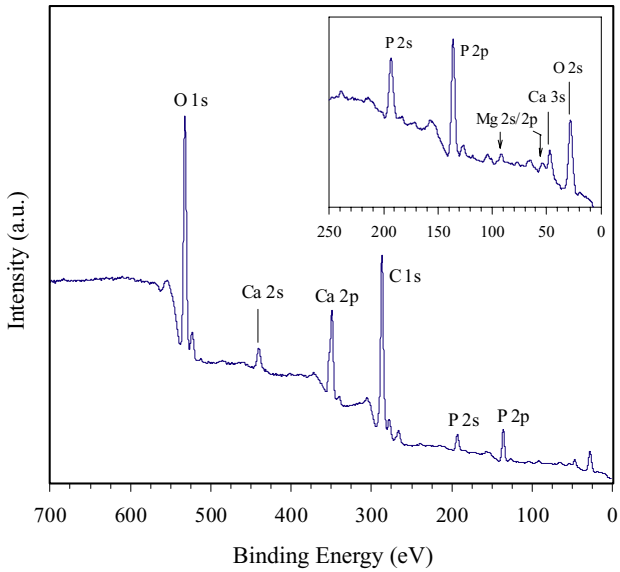

Fig. 2 XPS spectrum of the PHEMA hydrogel after incubation in SBF solution for 9 weeks

Table 1 XPS spectral data of the apatite layer formed on the surface of the PHEMA-based hydrogels after incubation in SBF solution for 5, 7 and 9 weeks. A. PHEMA, B. P(HEMA-co-EMA), C. P(HEMA-co-NVP) and D. P(HEMA-co-St)

Sample/ time	Mass conc. (%)					Mole ratio	
	C 1s	O 1s	Ca 2p	P 2p	Mg 2s	Ca/P	Mg/Ca
A5	42.24	31.02	14.46	10.27	1.65	1.09	0.19
A7	36.65	33.41	15.17	12.17	1.63	1.03	0.17
A9	37.35	33.10	16.17	11.08	2.11	1.12	0.21
B5	38.46	31.52	16.10	12.08	1.42	1.03	0.15
B7	38.80	34.37	14.69	10.94	0.83	1.04	0.09
B9	31.08	38.07	17.50	10.34	2.73	1.30	0.25
C5	41.19	35.33	12.24	9.25	1.84	1.02	0.24
C7	40.83	34.02	13.29	10.19	1.55	1.01	0.19
C9	41.51	36.44	12.25	8.10	1.35	1.17	0.18
D5	37.50	32.73	15.94	11.13	2.35	1.11	0.24
D7	37.84	32.12	15.83	12.01	2.00	1.02	0.21
D9	36.28	34.20	16.17	11.86	1.25	1.05	0.13

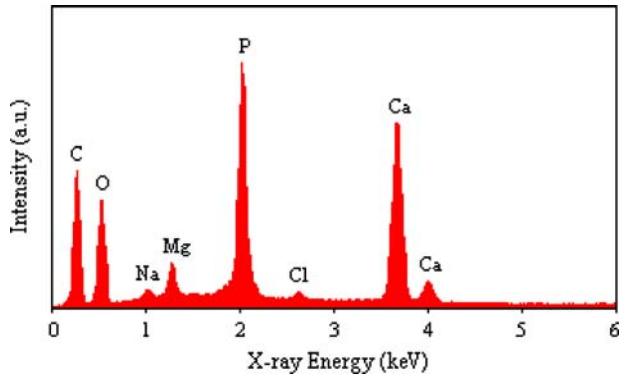

Fig. 3 EDS spectrum of the PHEMA hydrogel after incubation in SBF solution for 9 weeks

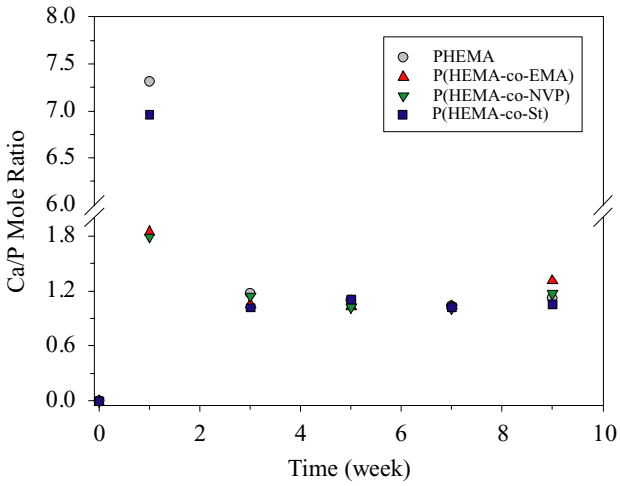

Fig. 4 Ca/P mole ratios for the deposits formed on the PHEMA-based hydrogels

and dicalcium phosphate dihydrate, DCPD ($CaHPO_4{\cdot}2H_2O$). Whitlockite usually has magnesium incorporated in its structure, but neither Cl^- nor CO_3^{2-} ions. DCPD is a biocompatible, biodegradable and osteoconductive material which can be found in fracture callus, bone and kidney stones. It is a metastable CaP and the most easily formed from a supersaturated calcium phosphate solution. At pH > 7, as in the case in SBF solution (pH 7–8), it converts to precipitated hydroxyapatite, PHAp [$Ca_{10-x}(HPO_4)_x(PO_4)_{6-x}(OH)_{2-x}$] [17, 18]. PHAp has a very complex chemistry, as it can have a Ca/P molar ratio which varies from 1.5 to 1.67, and even sometimes beyond this range [17–19]. PHAp with a Ca/P = 1.5 is often called calcium deficient hydroxyapatite (CDHA) or tricalcium phosphate, TCP [$Ca_3(PO_4)_2$]. PHAp crystals obtained by precipitation at pH > 7 have usually poor crystallinity.

At a higher level of supersaturation (as in the case of SBF solution), the formation of amorphous calcium phosphate, ACP [$Ca_3(PO_4)_2{\cdot}nH_2O$; n = 3–4.5; 15–20% H_2O] is favoured. However, since its solubility is higher than DCPD, ACP may not be the long-term stable form of CaP in the precipitates. The nature of ACP still provokes controversy. Some authors consider ACP to be an amorphous form of PHAp, but others report it to be OCP, TCP, DCPD, or Ca^{2+}, OH^- deficient apatites [17, 18].

Semi-quantitative XPS analysis for each of the elements present in the deposited layers formed on the samples that had been calcified for at least 5 weeks, showed that the Ca/P molar ratios lie between 1.0–1.3. The Mg/Ca molar ratios range from 0.1 to 0.25 (see Table 1). As the Mg/Ca molar ratios were mostly higher than the stoichiometric value for whitlockite (Mg/Ca = 0.11), some Mg^{2+} ions have replaced Ca^{2+} ions in the apatite lattice. Other types of CaP phases which are also possibly present in the deposits are OCP and TCP. Additionally, because of the presence of species such as Na^+, Mg^{2+} and CO_3^{2-} which can substitute for some of the ions of hydroxyapatite (e.g. Ca^{2+}; PO_4^{3-}; or OH^-) during equilibration in SBF solution, non-stoichiometric or defective hydroxyapatite is possibly formed. This particularly becomes apparent from a consideration of the Ca/P molar ratios in the early stages of calcification, i.e. for incubation times less than 5 weeks, where the ratio varied significantly from 1.0 to 7.5, as shown in Fig. 4. The observation of Ca/P molar

Table 2 The chemical structures of the units in the PHEMA-based hydrogels used in the study

Copolymer	F_{HEMA}	EWC (%)	Chemical structure
Control (PHEMA)	1.0	28.3	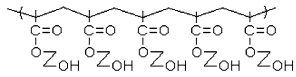
P(HEMA-co-EMA)	0.9	28.0	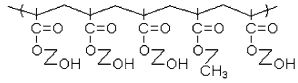
P(HEMA-co-NVP)	0.9	27.8	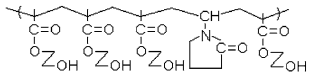
P(HEMA-co-St)	0.9	27.9	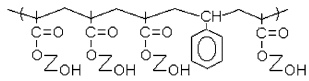

ratios that exceed 1.67 may be attributed to the substitution of PO_4^{3-} ions by CO_3^{2-} ions in the apatite lattice. This is also indicated in the infrared spectra that are discussed in more detail below. The lower Ca/P molar ratios (Ca/P < 1.67) observed at longer calcification times could be due to the substitution of some Ca^{2+} ions by Mg^{2+} ions, as mentioned above. The existence of carbonated apatite was confirmed by high resolution XPS analysis for C 1s and O 1s. In the C 1s spectrum (Fig. 5a), the main peak is associated with aliphatic carbon (C−H) and the other two peaks are due to the apatite carbonate carbon (C−O) and inorganic carbonate carbon, e.g. $MgCO_3$. In the O 1s spectrum (Fig. 5b), the oxygen peak for the carbonated apatite appears at a BE of 532.1 eV. The other two oxygen peaks correspond to P−O (531.3 eV) and P−O−H (533.3 eV) of DCPD and/or withlockite.

Taking into account that the Ca^{2+} ion has a strong tendency to chelate to oxygen atoms [20], and that PHEMA has 3 oxygen atoms in its unit structure, all of which are readily available for chelation, it was postulated that the extent of calcification of PHEMA may be lowered by decreasing the number of oxygen atoms in the matrix polymer through copolymerization. Table 2 shows how the relative number of polarizable oxygen atoms can be systematically reduced by copolymerization of HEMA with EMA, NVP or St. Although the data are somewhat scattered, the initial rate of the calcium accumulation determined by XPS is obviously reduced by decreasing the number of oxygen atoms in the matrix polymer (Fig. 6). At longer calcification times, it appears that the P(HEMA-co-NVP) has the lowest extent of calcification, yet it does not contain the smallest number of oxygen atoms. Similar results have also been demonstrated for the extent of calcification for copolymers of HEMA with EMA or 2-ethoxyethyl methacrylate (EEMA) [12]. Thus it is not yet clear whether there is any correlation between the

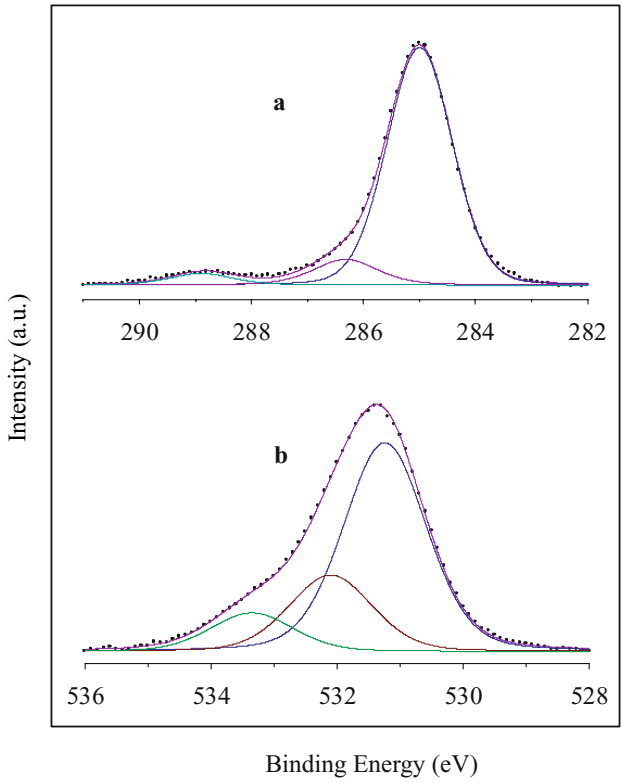

Fig. 5 High-resolution XPS spectra for C 1s (a) and O 1s (b) of the CaP deposits formed on the PHEMA hydrogel after 9 weeks calcification

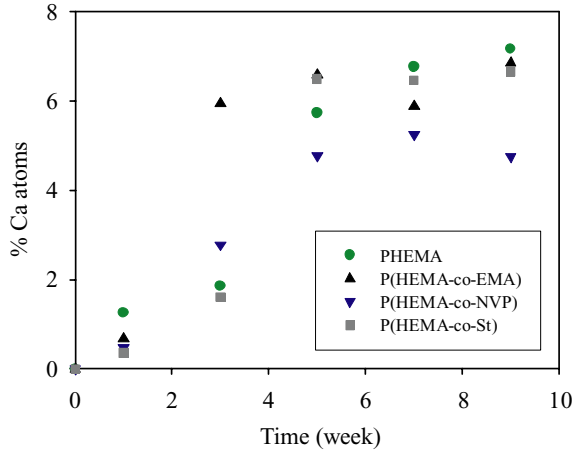

Fig. 6 The calcium content (measured by XPS technique) in the CaP deposits versus incubation time in SBF solution

extent of calcification of the hydrogel and the chemical structure of the matrix polymer.

Tanahashi and Matsuda [21] have suggested that the functional groups chemically attached to the surface of a gold substrate play an important role in the formation of an apatite layer on exposure to SBF. They found that a negatively charged functional group, such as $H_2PO_4^-$ and COO^-, strongly induced apatite formation. Other polar groups, including CONH, C(=O)O and OH and the protonated-NH_2 group, were found to be less potent. The CH_3 group, as a nonpolar or hydrophobic moiety, was claimed to totally prevent calcification. The works reported by Song et al. [22] and Filmon et al. [23, 24] also suggest that the ionic functional groups COO^- and $H_2PO_4^-$ strongly induced calcification in urea-treated PHEMA scaffolds and carboxymethylated PHEMA or alkaline phosphatase-treated PHEMA hydrogels. However, even though PHEMA hydrogels only have polar ester side chains and non-polar CH_3 groups, they are extensively calcified both in biological and abiotic calcifying media, such as SBF solution. What is more, the calcification of PHEMA hydrogels not only occurs on the surface, it also occurs inside the hydrogels, as evidenced by LM (Fig. 7b) and XPS (Fig. 7c) images. The extensive calcification of PHEMA and some other neutral hydrogel systems, such as PVA and PVP hydrogels [25], is considered to be due to a synergy between the high water content of the gels and the presence of the hydrophilic/hydrophobic domains of the matrix polymer. This synergy promotes the chelation of calcium and the formation of phosphate deposits. The process of calcification inside the hydrogel matrix occurs via the diffusion of ions into the hydrogels [26].

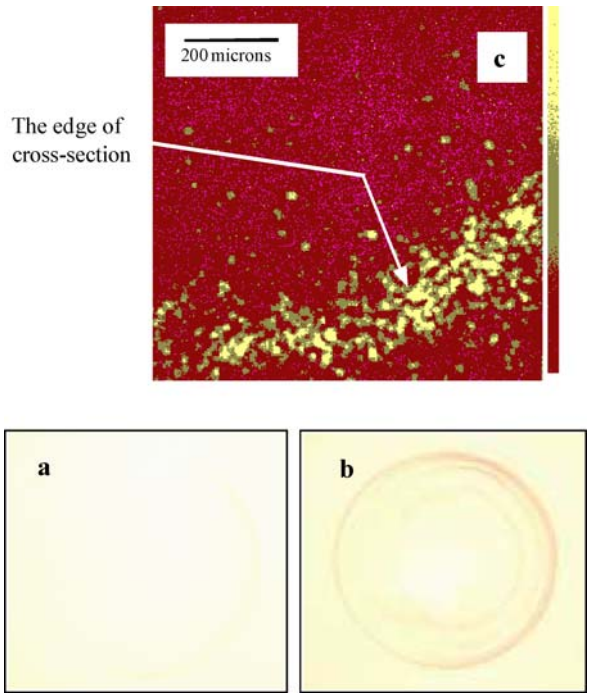

Fig. 7 The LM (a) before and (b) after, and XPS (c) images of the PHEMA hydrogels after 9 weeks calcification

The natures of the CaP phases in the hydrogels were examined either by FTIR-ATR or by FTIR studies using powdered samples in the form of KBr discs. The FTIR spectra of the CaP deposits are presented in Fig. 8, together with the spectra of sintered carbonated hydroxyapatite (CHAp) and DCPD for comparison. All of the samples showed spectral patterns similar to DCPD or CHAp (FTIR-ATR), suggesting that the type of CaP deposited varies from DCPD to CHAp. The characteristic phosphate bands at 1200−900 cm^{-1} and the carbonate bands at 1650−1300 cm^{-1} were observed in all of the spectra. The former band region is ascribed to the PO_4 group vibrational (ν_3) modes, while the latter band region is due to the CO_3 group vibrational (ν_3) modes [27–30]. The absence of a sharp peak at 3570 cm^{-1} due to the OH groups of HAp indicates that the CaP deposits do not contain significant amounts of HAp in a poorly crystalline or amorphous phase. The low intensity of the OH band for CHAp was reported to be due to a significant replacement of hydroxyl ions with carbonate ions [31], and the peak is partly masked by the broad H_2O absorption, as in the case of the CaP deposits formed in PHEMA-based hydrogels.

To examine more closely the development of the mineral phases during calcification, FTIR spectra (also given in Fig. 8), particularly in the spectral range of 2000 cm^{-1} to 450 cm^{-1}, were obtained for CaP deposited on the surface of PHEMA during incubation for 1 to 7 weeks. The band at 1645 cm^{-1} and the band at 793 cm^{-1} correspond to the vibrational modes of PO_4 groups in whitlockite and DCPD [29, 30]. These bands increase in intensity with incubation time. The peaks at 1550 cm^{-1} and 873 cm^{-1} can be ascribed to the bending modes of the carbonate group in a CHAp phase [29, 31] and/or a DCPD phase and/or $CaCO_3$ [32]. The presence of carbonate in the deposits is quite plausible as the concentration of carbonate in the SBF solution is relatively high. Incorporation of CO_3^{2-} ions as substitutes for PO_4^{3-} ions in the apatite lattice or the formation of $CaCO_3$, would both result in a Ca/P molar ratio that is higher than 1.67. The very weak peak at 1184 cm^{-1}, that is due to the PO_4 bending mode in OCP [29], increases in intensity with incubation time. The bands at 963 cm^{-1} and 945 cm^{-1} indicate the presence of HAp and TCP, respectively, and the bands at 562, 473 and 463 cm^{-1} are all due to the bending/vibrational modes of the PO_4 group of HAp [27–31].

The powder XRD patterns of PHEMA hydrogels after calcification in SBF solution for 9 weeks are presented in Fig. 9. The absence of any sharp and narrow peaks in the reflections confirms the previous results; namely that the CaP deposits are either amorphous or nano-crystalline precipitates. Note that the poorly resolved reflections from the CaP deposits are

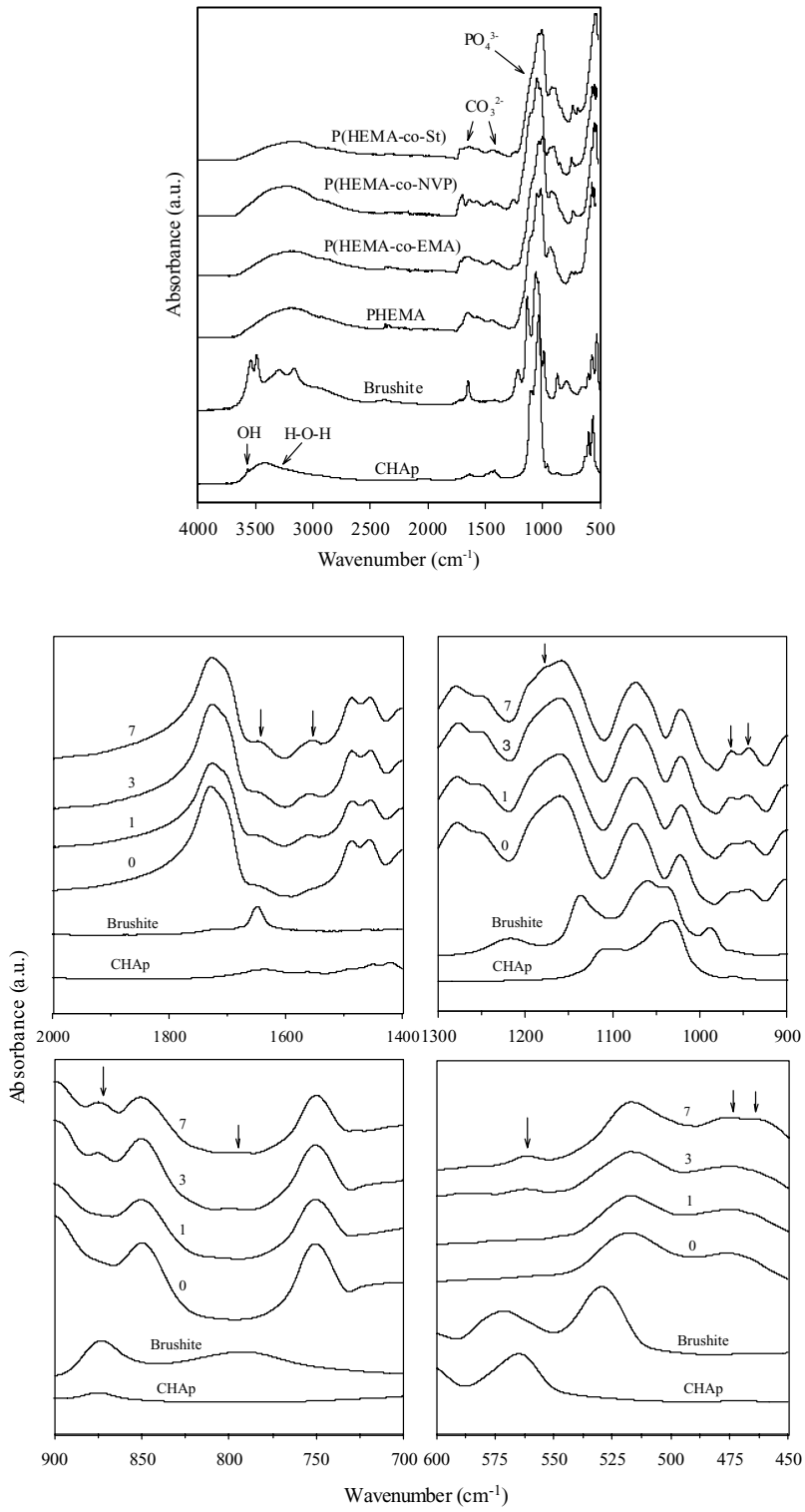

Fig. 8 ATR-FTIR spectra of the calcified (7 weeks) PHEMA-based hydrogels and FTIR spectra of the PHEMA hydrogels after incubation in SBF solution for: 0 (0 week), 1 (1 week), 3 (3 weeks) and 7 (7 weeks)

partially overlapped by reflections from the PHEMA. As a result, it is difficult to discern all of the peaks associated with the CaP phases present. The broad and weak peak at $2\theta \approx 29^\circ$ can be ascribed to a DCPD reflection (11-2) [33], as it is closely matches the ICSD pattern of 01-072-07130 for DCPD. Based on the ICSD pattern of 01-070-2064 for whitlockite and the ICSD pattern of 00-021-0145/01-084-1998 for CHAp/HAp, the peak at 2θ between 31° and 34°, which is the main resolved peak in the XRD pattern for PHEMA+CaPs, is probably due to the reflections of whitlockite (217 and 128) [34]

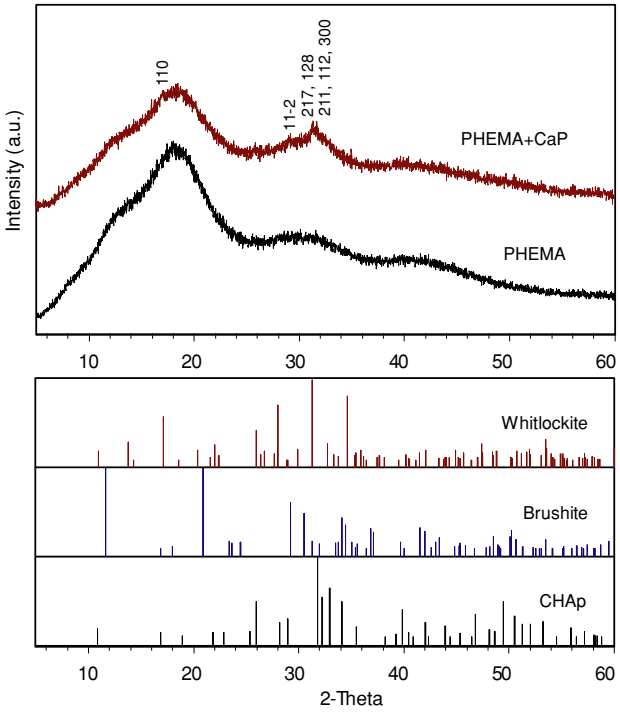

Fig. 9 XRD spectra of the PHEMA hydrogels before and after 9 weeks incubation in SBF solution

or CHAp/HAp (211, 112 and 300) [35, 36]. Additionally, the small and broad peak at $2\theta \approx 17^{\circ}$ is very close to the whitlockite reflection (110). Thus the XRD results are consistent with the results obtained by SEM, EDS/XPS and FTIR measurements, which show that the CaP deposits formed in SBF are comprised mainly of whitlockite-type apatite and DCPD, which are the precursors of HAp. It appears that the transformation of CaP deposits into HAp is hindered by the presence of Mg. This stabilization effect of Mg on CaP deposits is well known in biological calcification [19, 37].

4 Conclusions

PHEMA-based hydrogels have been shown to calcify both on the surface and in the interior of the hydrogels during incubation in SBF solution. The calcification process occurs predominantly through spontaneous precipitation of CaP, which forms mainly an amorphous or a nanocrystalline phase of whitlockite-type apatite and DCPD. These are the precursors of HAp. The effect of the chemical structure (reducing the number of oxygen atoms in the copolymers on the degree of calcification) was found to play an important role only in the initial stages of calcification. At longer calcification times, there was no significant effect of chemical structure or oxygen content on the formation of CaP deposits.

Acknowledgments The authors would like to acknowledge the Australian Research Council for the financial support through out the project. Z also thanks The University of Queensland for the IPRS and UQGSS scholarships. The assistance received from Dr. Barry Wood for XPS, Dr. Llewellyn Rintoul for ATR-FTIR, Mr. John Nailon, Mr. Kim Sewel and Mr. Ron Rush for SEM-EDS, Dr. Anne Kemp for staining, and Ms. Anya Josefa Yago for XRD measurements is gratefully acknowledged.

References

1. E. BONUCCI, *J. Bone Miner. Metab.* **20** (2002) 249.
2. S. VIJAYASEKARAN, T. V. CHIRILA, T. A. ROBERTSON, X. LOU, J. H. FITTON, C. R. HICKS and I. CONSTABLE, *J. Biomater. Sci. Polym. Edn.* **11** (2000) 599.
3. T. KOKUBO, *J. Non-Cryst. Solids* **120** (1990) 138.
4. L. WERNER, D. J. APPLE, M. ESCOBAR-GOMEZ, A. OHRSTROM, B. B. CRAYFORD, FRACO, R. BIANCHI and S. K. PANDEY, *Ophthalmology* **107** (2000) 2179.
5. L. WERNER, D. J. APPLE, M. KASKALOGLU and S. K. PANDEY, *J. Cataract. Refract. Surg.* **27** (2001) 1485.
6. P. J. BUCHER, E. R. BUCHI and B. C. DAICKER, *Arch. Ophthalmol.* **113** (1995) 143.
7. S. L. MCARTHUR, K. M. MCLEAN, H. A. W. ST. JOHN and H. J. GRIESSER, *Biomaterials* **22** (2001) 3295.
8. O. MORADI, H. MODARRESS and M. NAROOZI, *J. Colloid and Interface Sci.* **271** (2004) 16.
9. N. VYAVAHARE, M. OGLE, F. J. SCHOEN and R. J. LEVY, *Am. J. Pathol.* **155** (1999) 973.
10. F. J. SCOEN and R. J. LEVY, in "Biomaterials Science" (Elsevier Inc., San Diego, 2004) p. 439.
11. T. V. CHIRILA, Z. GRIDNEVA, D. A. MORRISON, C. J. BARRY, C. R. HICKS, D. J. T. HILL, A. K. WHITTAKER and ZAINUDDIN, *J. Mater. Sci.* **39** (2004) 1861.
12. T. V. CHIRILA, D. A. MORRISON, Z. GRIDNEVA, A. J. A. GARCIA, S. T. PLATTEN, B. J. GRIFFIN, ZAINUDDIN, A. K. WHITTAKER and D. J. T. HILL, *J. Mater. Sci.* **40** (2005) 4987.
13. D. D. PERRIN and W. L. F. ARMAREGO (Pergammon Press, New York, 1988) p. 12.
14. A. C. TAS, *Biomaterials* **21** (2000) 1429.
15. E. SAIZ, M. GOLDMAN, J. M. GOMES-VEGA, A. P. TOMSIA, G. W. MARSHALL and S. J. MARSHALL, *Biomaterials* **23** (2002) 3749.
16. F. ABBONA and A. F. ANGELA, *J. Crystal Growth* **104** (1990) 661.
17. J. P. BARONE, in "The Role of Calcium in Biological Systems" (CRC Press Inc., Boca Raton, 1982) p. 27.
18. M. BOHNER, *Injury, Int. J. Care Injured* **31** (2000) S-D37.
19. A. KRAJEWSKI and A. RAVAGLIOLI, in "Integrated Biomaterials Science" (Kluwer Academic/Plenum Publishers, New York, 2002) p. 189.
20. B. A. LEVINE and R. J. P. WILLIAMS, in "The Role of Calcium in Biological Systems" (CRC Press, Boca Raton, 1982) p. 3.
21. M. TANAHASHI and T. MATSUDA, *J. Biomed. Mater. Res.* **34** (1997) 305.
22. J. SONG, E. SAIZ and C. R. BERTOSZZI, *J. Am. Chem. Soc.* **125** (2003) 1236.
23. R. FILMON, M. F. BASLE, A. BARBIER and D. CHAPPARD, *J. Biomater. Sci. Polym. Edn.* **11** (2000) 849.
24. R. FILMON, F. GRIZON, F., M. F. BASLE and D. CHAPPARD, *Biomaterials* **23** (2002) 3053.
25. ZAINUDDIN, D. J. T. HILL, A. K. WHITTAKER, K. STROUNINA and T. V. CHIRILA, *Polym. Preprints* **42** (2004) 368.

26. ZAINUDDIN, T. V. CHIRILA, D. J. T. HILL and A. K. WHITTAKER, *J. Molecul. Struct.* **739** (2005) 199.
27. B. O. FOWLER, E. C. MORENO and W. F. BROWN, *Arch. Oral Biol.* **11** (1966) 477.
28. I. REHMAN and W. BONFIELD, *J. Mater. Sci. Mater. Med.* **8** (1997) 1.
29. S. KOUTSOPOULOS, *J. Biomed. Mater. Res.* **62** (2002) 600.
30. M. C. CHANG and J. TANAKA, *Biomaterials* **23** (2002) 4811.
31. C. KLEIN, F. A. MULLER and P. GREIL, *Key Eng. Mater.* **254/256** (2004) 391.
32. P. R. CHRISTENSEN, J. L. BANDFIELD, V. E. HAMILTON, D. A. HOWARD, M. D. LANE, J. L. PIATEK, S. W. RUFF and W. L. STEFANOV, *J. Geophys. Res.* **105** (2000) 9735.
33. N. A. CURRY and D. W. JONES, *J. Chem. Soc.* A **1971** (1971) 3725.
34. R. GOPAL and C. CALVO, *Can. J. Chem.* **52** (1974) 1155.
35. N. BROPHY, *Am. Mineral* **53** (1968) 445.
36. J. M. HUGHES, M. CAMERON and K. D. CROWLEY, *Am. Mineral* **74** (1989) 870.
37. H. FLEISCH, in "Biological Mineralization and Demineralization" (Springer-Verlag, Berlin, 1982) p. 233.